Journal of Alloys and Compounds 508 (2010) 133–140

Contents lists available at ScienceDirect

Journal of Alloys and Compounds

journal homepage: www.elsevier.com/locate/jallcom

Composition and phase control of Ni/NiO nanoparticles for photocatalytic degradation of EDTA

F.A. Harraz*, R.M. Mohamed, A. Shawky, I.A. Ibrahim

Nanostructured Materials and Nanotechnology Division, Central Metallurgical Research and Development Institute, 1 El-Felezate Street, El-Tebbin, P.O. Box 87, Helwan, Cairo 11421, Egypt

ARTICLE INFO

Article history:
Received 29 March 2010
Received in revised form 5 August 2010
Accepted 6 August 2010
Available online 18 August 2010

Keywords:
Sol–gel technique
Nanoparticles
Ni/NiO
EDTA
Photodegradation

ABSTRACT

A sol–gel process followed by a calcination treatment was employed to synthesize magnetic Ni/NiO nanoparticles. The as-formed particles were characterized using XRD, TEM, UV–vis, surface area and VSM. The XRD results show that the patterns of the product synthesized using 1:1, 1:2, and 1:3 molar ratio of nickel nitrate/citric acid composed of a mixture of NiO and Ni, whereas the patterns recorded for 2:1 and 3:1 molar ratio exhibited a single NiO phase. All the prepared samples are in the form of nanoparticles with sizes locate in the range of 33 up to 118 nm for the samples prepared by different molar ratios. The photocatalytic tests were conducted for degradation of EDTA. The results show that the EDTA removal efficiency is 99.9% at 3×10^{-3} M EDTA concentration. The reaction of Ni/NiO with EDTA follows first order kinetics with respect to EDTA. The rate constants and $t_{1/2}$ for Ni/NiO at 0.4 g/l catalyst/EDTA solution ratio were, respectively 460 min^{-1}, 15.1 min.

1. Introduction

Ethylenediamminetetraactetic acid (EDTA) is a domestic and industrial water contaminant. It is widely used as a decontaminating agent in nuclear industry. The presence of EDTA in radioactive liquid waste can cause complexation of some of the target precipitant cations resulting in interference in their removal by conventional treatment processes such as chemical precipitation or ion exchange [1,2]. EDTA is not easily biodegradable [3], rarely degradable by chlorine [4], hardly retained by activated carbon fibres and resistant to ozone treatment [5,6]. Accordingly, it is a crucial step to perform a pretreatment step for the removal of EDTA for a better treatment of the liquid wastes.

Recently, advanced oxidation method based on photocatalysis has been employed successfully for degradation of organic pollutants [7–10]. For example, several works dedicated to the photocatalytic degradation of reactive brillian red using boron-doped titania [11], catalytic decomposition of methylene blue on doped-TiO_2 nanoparticles [12,13], photocatalytic activity of nanostructured ZnO films for decolorization of malachite green [14] are recently reported. The main advantage of applying such a technique is its capability to convert the organic pollutants into nontoxic species such as CO_2 and H_2O. Another big advantage for this approach is the fact that no further separation processes are needed. Heterogeneous photocatalysis which is a category of advanced oxidation method is therefore a promising method by which a semiconductor catalyst under UV irradiation is able to mineralize EDTA, for instant. In heterogeneous photocatalysis, $OH^{\bullet}$ radicals, already generated by UV light, are the essential species in degradation of EDTA. This means, using this method, chemical oxidants can be released in water as the result of catalyst irradiation. In reality, redox processes are likely taking place at the catalyst/solution interface as long as the semiconductor is irradiated by a wavelength higher enough than the band gap of the catalyst. Absorption of photons generates electron–hole pairs on the catalyst surface which in turn can reduce or oxidize the organic materials present in aqueous solutions. Reaction of holes with water can lead to the formation of oxidizing radicals which can attack EDTA and transform it to CO_2 and H_2O species.

Most of previous reports devoted to remove EDTA from water using heterogeneous catalysis have been conducted using TiO_2 semiconductor catalyst irradiated with wide range of spectral lamps [15–21]. This means, to date there are challenges for developing the controlling parameters of the heterogeneous photocatalysis, including developing new types of catalyst, deep investigation on catalyst operation and its performance evaluation and other relevant aspects as well. This in turn should enable advances in such emerging area of catalysis.

On the other hand, NiO has recently received increased attention due to its applications in a wide range of fields, including catalysis [22], electrochromic films [23–26], fuel cell electrodes [27,28], gas sensors [29,30], and smart windows [31–33]. Various meth-

* Corresponding author. Tel.: +20 2 25010 640, fax: +20 2 25010 639.
E-mail addresses: fharraz@cmrdi.sci.eg, fharraz68@yahoo.com (F.A. Harraz).

0925-8388/$ – see front matter © 2010 Elsevier B.V. All rights reserved.
doi:10.1016/j.jallcom.2010.08.027

ods have been known for synthesizing NiO including calcinations of nickel compound in air at elevated temperature 1273 K, physical and chemical vapor deposition and sol–gel process [24,34,35].

For example, Jiao et al. have recently reported a dip coating process combined with sol–gel method to fabricate NiO films [24]. Wang et al. have synthesized NiO nanorods by a thermal decomposition technique [36]. NiO nanowires with a polycrystalline nature have also been synthesized by an electrochemical deposition approach [37], while single cubic crystal NiO nanowires have been fabricated by means of a wet chemical method [38] and by an oxidation route in a molten salt [39]. Importantly, some other authors have reported and used NiO as a photocatalyst for degradation of phenol [40]. Actually, the band gap of NiO is higher than TiO_2, but the degradation process is a bit higher than TiO_2. The main reason for the increase in degradation efficiency in case of NiO is the release of lattice oxygen by which super-oxide radicals are formed which greatly enhance degradation of phenol [40]. Furthermore, it was reported that NiO formed on $AgNbO_3$ surface and Ag-doped $NiTiO_3$ could enhance the photocatalytic decomposition of methylene blue [41,42]. As a recent report, a photocatalyst $LaNiO_3$ with perovskite structure was used successfully for methyl orange degradation [43].

However, a definite understanding of the limits of NiO formation and its phase and morphology control is still lacking. To better understand this, we report a simple sol–gel method followed by a calcination process to synthesize Ni/NiO nanoparticles. A detailed investigation was conducted in which the nanostructure phase and morphology were correlated to a systematic variation in operating parameters, with focusing to control the phase formation, and evaluate the applicability of the as-formed catalyst for the degradation of EDTA.

2. Experimental details

2.1. Materials preparation and characterization

The sol–gel method was employed as follows: 5 g $Ni(NO_3)_2{\cdot}6H_2O$ and x g citric acid (x = 1.8, 3.61, 5, 6.9 and 9.025 g) were used to prepare different molar ratios from $Ni(NO_3)_2{\cdot}6H_2O$:citric acid, mainly 2:1, 1:1, 1:3, 3:1 and 1:2. The precursor was dissolved in 100 ml pure alcohol until a clear mixed solution is formed; and then the solution was kept at 120 °C in an oven until the alcohol entirely evaporated and a green paste was obtained. After the sol–gel process, the paste was placed into a tube furnace, and calcined at 750 °C for 5 h in air. The products were then characterized using XRD, TEM, UV–vis, surface area and VSM. The magnetic properties of the produced powders were measured, at room temperature, using a vibrating sample magnetometer (VSM; 9600-1 LDJ, USA) in a maximum applied field of 15 kOe. From the obtained hysteresis loops, the saturation magnetization (M_s) and coercivity (H_c) were determined. X-ray diffraction (XRD) patterns of calcined catalysts were measured using Rigaku RINT 2000. A Perkin-Elmer Lambda 800 UV/vis spectrometer was used to determine the particle band-gap profile. During measurement the samples were dispersed in aqueous systems placed into plastic cuvettes for measurement. N_2-adsorption measurement was carried out at 77 K using Nova 2000 series, Chromatech. Prior to analysis, the samples were outgased overnight at 250 °C. The morphology and particle size of the prepared samples were examined by transmission electron microscopy (TEM; Hitachi H-9500 operated at 300 kV).

2.2. Photocatalytic tests

The photoactivity tests were carried out in a cylindrical Pyrex glass reactor containing different catalyst loadings in 250 ml of aqueous solution of 5×10^{-3} M EDTA at 30 °C for 60 min. A 150 W medium pressure Hg lamp (254 nm) immersed within the photoreactor was used. The EDTA was determined by a comlexometric titration with Zn^{2+} standard solution [44]. The removal efficiency of EDTA was calculated by applying the following equation:

$$\text{removal efficiency} = \left[\frac{C_0 - C}{C_0}\right] \times 100\%$$

where C_0 is the original EDTA content and C the retained EDTA in solution. Prior to the photocatalytic tests, fresh solutions of 250 ml containing EDTA were adjusted to a certain pH, and the catalyst was suspended at 0.4 g/l concentration. Suspensions were kept in dark and continuously stirred at 30 °C for 60 min.

Table 1
Relation between nickel nitrate/citric acid molar ratios and the percentage of the formed phases, band gap, and photocatalytic degradation of EDTA.

Nickel nitrate/citric acid molar ratio	% of formed phase		Direct band gap (eV)	Photocatalytic degradation of EDTA (%)
	NiO	Ni		
1:1	46	54	3.53	63.7
2:1	100	0	3.44	88.8
3:1	100	0	3.42	94.5
1:2	70	30	3.47	85.8
1:3	18	82	3.60	48.9

3. Results and discussion

3.1. Effect of nickel nitrate/citric acid molar ratio

A series of experiments has been carried out using different nickel nitrate/citric acid molar ratio, mainly 2:1, 1:1, 1:3, 3:1 and 1:2. The as-formed products were characterized using XRD, surface area, TEM, and UV–vis. The photocatalytic tests were consequently performed for degradation of EDTA.

3.2. X-ray diffraction

Fig. 1 displays the XRD patterns of the samples prepared using different nickel nitrate/citric molar ratios as 1:1, 1:2, 2:1, 1:3 and 3:1. The patterns of the product synthesized at 1:1, 1:2, and 1:3 molar ratio indicate that a mixture of NiO and Ni existed, whereas the patterns of the product synthesized at 2:1 and 3:1 molar ratio reveals a single NiO phase. From the patterns, it can be seen that three distinct diffraction peaks at $2\theta = 37°$, 43° and 63° are observed for nanosized NiO samples. These peak positions correspond well with the three most intense peaks (1 1 1), (2 0 0), (2 2 0) of pure NiO. Weaker intensity peaks detected at $2\theta = 75°$ and 79° can be indexed, respectively to (3 1 1) and (2 2 2) crystal plans of NiO. The observed diffraction peaks at $2\theta = 44°$, 52°, and 76° are assigned to (1 1 1), (2 0 0) and (2 2 0) of Ni, respectively. It is worth to note that the peak positions are not shifted, but the shapes are broader than the standard peaks, which can be essentially related to the nanosize of as-synthesized particles. Table 1 shows the effect of nickel nitrate/citric acid molar ratio on the percentage and the crystallite size of the as-formed phases. The results show that increasing the nickel nitrate/citric acid molar ratio in the order of 1:1, 2:1 and 3:1, led to increasing the percentage of NiO in the formed phase from 46, 100 and 100, respectively. However, the above trend of increasing nickel nitrate/citric acid molar ratio was found to decrease the crystallite size (calculated by Scherer equation [45]) from 118, 94.3 and 75.6 nm, respectively. On the other hand, by decreasing the nickel nitrate/citric acid molar ratio in the order of 3:1, 1:2 and 1:3, one can observe a decrease of NiO% in the formed phases from 100, 70 and 18%, respectively.

Citrate ions can play multiple roles in the synthesis process, including a reducing agent, a stabilizer and a complex agent. Citrate ions could form a nickel complex with nickel ions in solution. The formation of Ni(II)–citrate complexes depends essentially on the molar ratio between Ni(II) and citric acid. Different molar ratios between nickel ions and citric acid can greatly influence the reaction rate and the final phases as well as the particle size. The reducing ability of citrate ions is a function of concentration. Our findings indicated that, as the concentration of citric acid increases in solution, the amount of Ni metal phase increases. Low concentration of citrate ions favors the formation of NiO. A complete reaction mechanism needs further spectrometry and kinetic analysis.

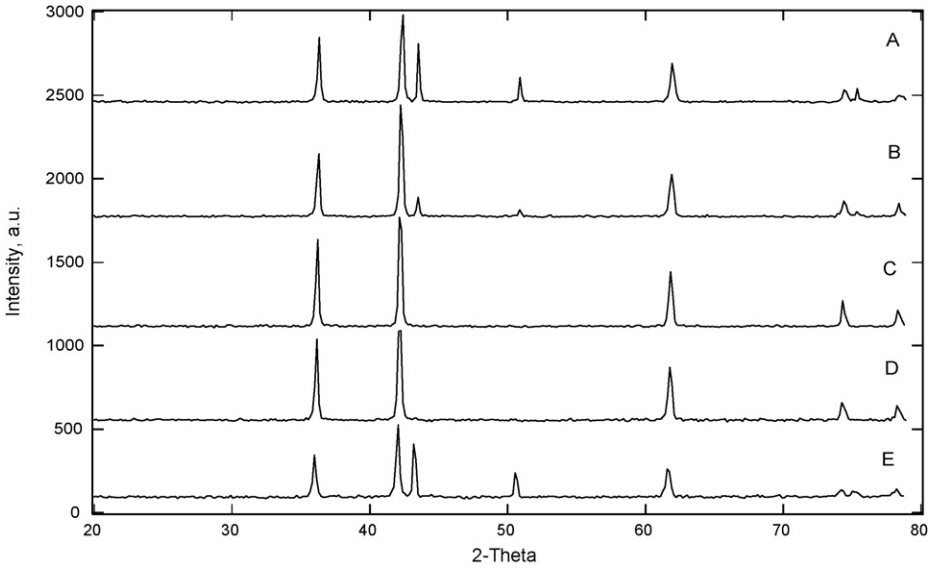

Fig. 1. XRD of the prepared samples obtained by different nickel nitrate/citric acid molar ratios; nickel nitrate/citric acid molar ratio: (A) 1:1, (B) 1:2, (C) 2:1, (D) 3:1 and (E) 1:3.

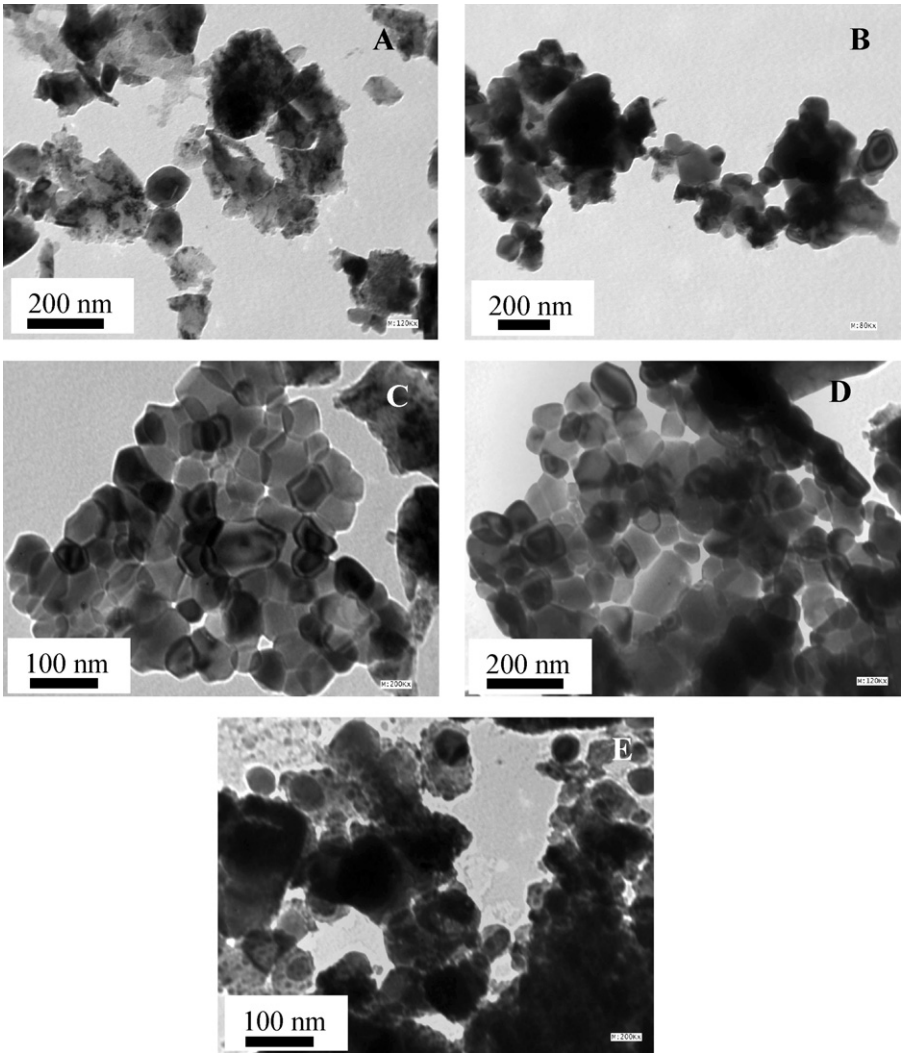

Fig. 2. TEM images of the prepared samples obtained by different nickel nitrate/citric acid molar ratios; nickel nitrate/citric acid molar ratio: (A) 1:1, (B) 1:2, (C) 2:1, (D) 3:1 and (E) 1:3.

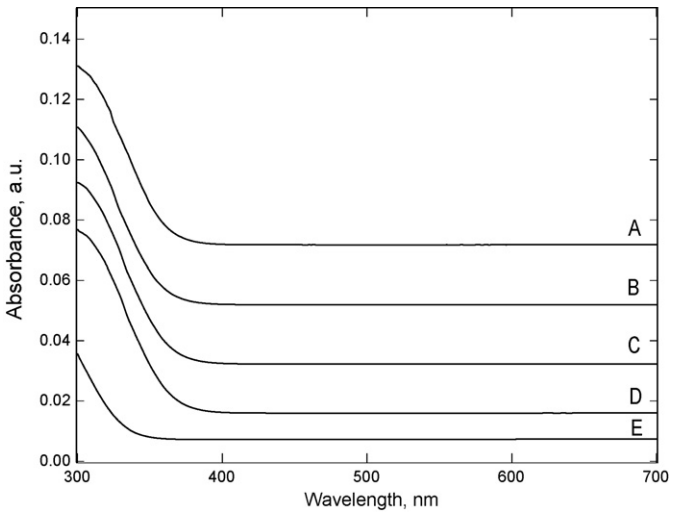

Fig. 3. UV–vis of the prepared samples obtained by different nickel nitrate/citric acid molar ratios; nickel nitrate/citric acid molar ratio: (A) 1:1, (B) 1:2, (C) 2:1, (D) 3:1 and (E) 1:3.

3.2.1. Transmission electron microscopy (TEM)

Fig. 2 shows the TEM images of the prepared samples using different molar ratios of nickel nitrate/citric acid. The micrographs show that all the prepared samples are in the form of nanoparticles with sizes in the range of 33–97, 48–80, 28–50, 42–119 and 40–90 nm for samples prepared using 1:1, 1:2, 2:1, 3:1 and 1:3 molar ratios, respectively. In complementary to the above XRD spectra of as-formed samples, it can be realized that the nanoparticles are formed as a mixture of hexagonal and cubic in case of 1:1, 1:2 and 1:3 molar ratio, whereas they are hexagonal in case of 2:1 and 3:1 molar ratios.

3.2.2. UV–vis

The DR-UV spectra of the samples prepared by different nickel nitrate/citric acid molar ratios are shown in Fig. 3. Inspection of the spectra reveals the existence of absorption signals around 365 nm, which is likely related to NiO. The origin of such absorption is attributed to intra-3^d transition of Ni^{2+} in the hexagonal structure of NiO [46,47]. For the samples prepared using different nickel nitrate/citric acid molar ratios, one can observe that the absorption signals would gradually shift to shorter wavelength with moving from sample (A) to sample (E). An estimate of the optical band gap is obtained using the following equation:

$$\alpha(h\gamma) = A(h\gamma - Eg)^{m/2}$$

where A is a constant, α is the absorption coefficient, and m equals 1 for a direct transition. The energy intercept of a plot of $(\alpha h\gamma)^2$ vs. $(h\gamma)$ yields Eg for a direct transition [48]. The band-gap value usually reported for NiO phase is 3.5 eV [35]. However, these values are generally influenced by the synthesis method, the existence of impurities doping the crystalline network and the average crystal size of the semiconductor. The band-gap values calculated for as-formed samples are presented in Table 1. The results show a gradual narrowing of the band gap with increment of nickel nitrate/citric acid molar ratio, which in turn would increase the absorbency in the visible light region.

3.2.3. Surface area measurement at different nickel nitrate/citric acid molar ratios

The N_2 adsorption–desorption measurement at a liquid N_2 temperature of −196 °C was used to study mesoporosity and textural properties of the synthesized NiO nanoparticles. Fig. 4 depicts the as-recorded N_2 adsorption–desorption isotherm. The isotherm shows a typical type IV sorption behavior with type H2 hysteresis loop, representing the mesoporous structure according to the classification of IUPAC [49]. The apparent step in the adsorption branch combined with the sharp decline in the desorption branch is an obvious indication of mesoporosity. An abrupt increase in adsorption volume of adsorbed N_2 was observed and located in the P/P_0 value greater than 0.6. This sharp increase is generally associated with the capillary condensation, indicating the good homogeneity of the sample and fairly small pore size since the P/P_0 position of the inflection point is related to the pore size. From the N_2 adsorption–desorption, TEM and XRD analysis, the as-synthesized Ni/NiO possesses nanocrystalline mesoporous structure. The textural properties of the nanocrystalline mesoporous Ni/NiO samples are given in Table 2. The results show that BET surface area of 123, 107, 61, 31 and 26 $m^2\ g^{-1}$ with total pore volume of 0.16, 0.34, 0.93, 0.34 and 0.46 $cm^3\ g^{-1}$ for nickel nitrate/citric acid molar ratio equal 3:1, 2:1, 1:2, 1:1 and 1:3, are achieved respectively.

3.2.4. Effect of nickel nitrate/citric acid molar ratio on photocatalytic degradation of EDTA

A series of experiments has been conducted to study the effect of nickel nitrate/citric acid molar ratio on EDTA removal efficiency under the following conditions: 0.4 g/l catalyst/EDTA solution ratio; 5×10^{-3} M EDTA; 1 h reaction time and at pH 3. The results indicate that increasing nickel nitrate/citric acid molar ratio in the order 1:2, 2:1 and 3:1 leads to increasing EDTA removal efficiency from 85.8, 88.8 and 94.5%, respectively. This is attributed to an increase in the % of NiO from 70, 100 and 100% and surface area from 61, 107 and 123 m^2/g, respectively and a decrease in the band gap in the order of 3.47, 3.44 and 3.42 eV, respectively. However, by decreasing the nickel nitrate/citric acid molar ratio in the order 1:1, 1:2, and 1:3, one can find a significant change in EDTA removal efficiency with the following values: 63.7, 85.8 and 48.9, respectively. From the photocatalytic point of view, the optimum condition of nickel nitrate/citric acid molar ratio is 3:1 at which the prepared catalyst has 123 m^2/g BET surface area, 3.42 eV band gap, 100% NiO and 94.5% EDTA removal efficiency. However, for the sake of achieving a magnetic photocatalyst, the sample with nickel nitrate/citric acid molar ratio of 1:2 at which the prepared catalyst has 61 m^2/g BET surface area, 3.47 eV band gap, 70% NiO,

Table 2
Textural, surface and morphology of prepared samples by different molar ratios of nickel nitrate/citric acid.

Nickel nitrate/ citric acid	S_{BET} (m^2/g)	S_t (m^2/g)	V_m (mL/g)	V_P (mL/g) Total	r (Å)	$S_{ex.}$ (m^2/g)	V_P (mL/g) micro	V_P (mL/g) meso	V_P (%) micro	V_P (%) meso	S_{micro} (m^2/g)	S_{meso} (m^2/g)	C_{BET}
3:1	123.1	74.98	28.15	0.16	33.38	193.46	34.77	0.09	0.07	59.43	40.57	58.52	39.95
2: 1	107.5	24.49	24.59	0.34	79.30	108.71	39.58	0.05	0.29	16.05	83.95	13.77	79.98
1:2	61.00	70.00	14.00	0.930	381.00	33.00	0.003	0.930	0.33	100.00	0.160	49.00	25.00
1:1	31.00	40.00	7.00	0.340	275.00	31.00	0.010	0.320	5.70	94.00	9.00	23.00	11.00
1:3	26.00	30.00	1.50	0.460	443.00	35.00	0.080	0.370	18.00	82.00	7.00	17.00	6.00

S_{BET}: BET surface area; S_t: surface area derived from V_{l-t} plots: S_{micro}: surface area of micropores; V_{micro}: pore volume of micropores; S_{meso}: surface area of micropores; r: mean pore radius; $S_{ex.}$: external surface area; V_P: total pore volume; V_{meso}: pore volume of mesopores.

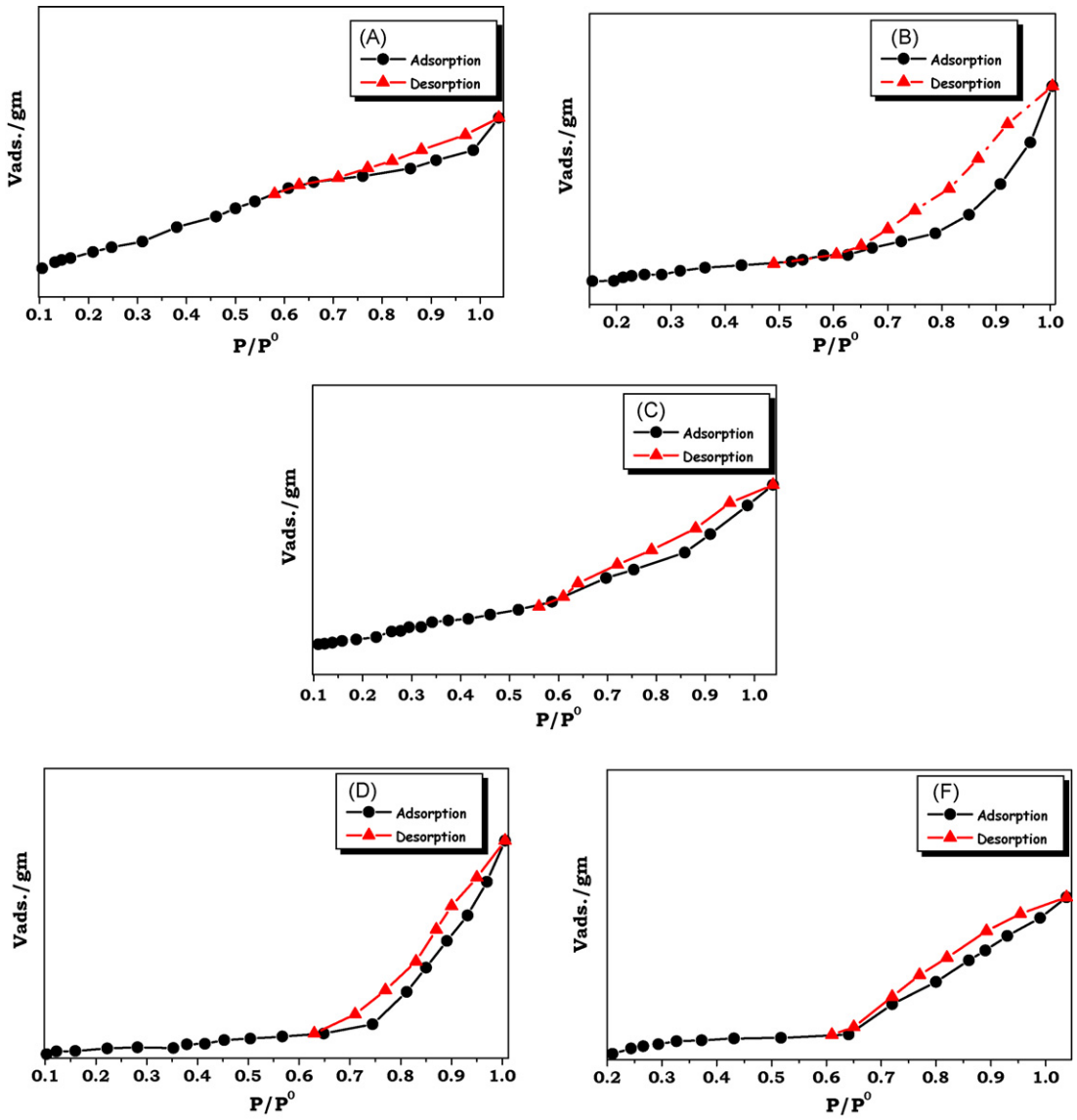

Fig. 4. N_2 adsorption–desorption isotherm of the prepared Ni/NiO nanoparticles prepared by different nickel nitrate/citric acid molar ratios; nickel nitrate/citric acid molar ratio: (A) 1:1, (B) 1:2, (C) 2:1, (D) 3:1 and (F) 1:3.

30% Ni and 85.8% EDTA removal efficiency is selected for further investigation.

3.3. Effect of calcination temperature

The optimum catalyst prepared using 1:2 nickel nitrate/citric acid molar ratio is subsequently calcined at different temperatures ranging from 550 to 850 °C. The samples after heat treatment were characterized using XRD, surface area, TEM. Then, the photocatalytic tests were carried out for degradation of EDTA to understand the catalytic performance of our catalyst before and after calcination.

3.3.1. Phase, morphology and magnetic properties evaluation

Fig. 5 shows the XRD patterns of calcined samples prepared at different temperatures, mainly 550, 650, 750 and 850 °C. The XRD patterns of samples treated at 550, 650, and 750 °C calcination temperatures revealed a mixture of NiO and Ni phases; however the pattern related to the sample synthesized at 850 °C shows a single phase of NiO with a good crystalline state. Table 3 shows the effect of calcination temperature on the percentage and the crystallite size of the formed phases. As can be seen, the crystallite size increases gradually (61.8, 90.4, 95.0 and 101.7 nm) as the calcination temperature increases, respectively from 550, 650, 750 and 850 °C. It is believed that higher temperature enhances the growth of the formed clusters, which results in faster growth speed.

Fig. 6 shows the TEM images of as-prepared samples that were subjected to heat treatment at different calcination temperatures, mainly 550, 650, 750 and 850 °C. The images reveal the formation of nanoparticles with sizes ranging from 15 to 30, 15 to 65, 50 to 70 and 70 to 120 nm for the samples treated at 550, 650, 750 and 850 °C, respectively; note the different scale bars of TEM image D. It can be realized that the average particle size increases with calcination temperature. According to the XRD results, it can be realized that the nanoparticles are a mixture of hexagonal and cubic in case of 550, 650, and 750 °C, whereas a hexagonal NiO is achieved in case of 850 °C calcination temperature.

The magnetic properties recorded by the vibrating magnetometer at a room temperature for different produced catalysts thermally treated from 550 to 850 °C are listed in Table 4. The results show that the as-formed catalyst treated at 550 °C calcination temperature has high saturation magnetization, high

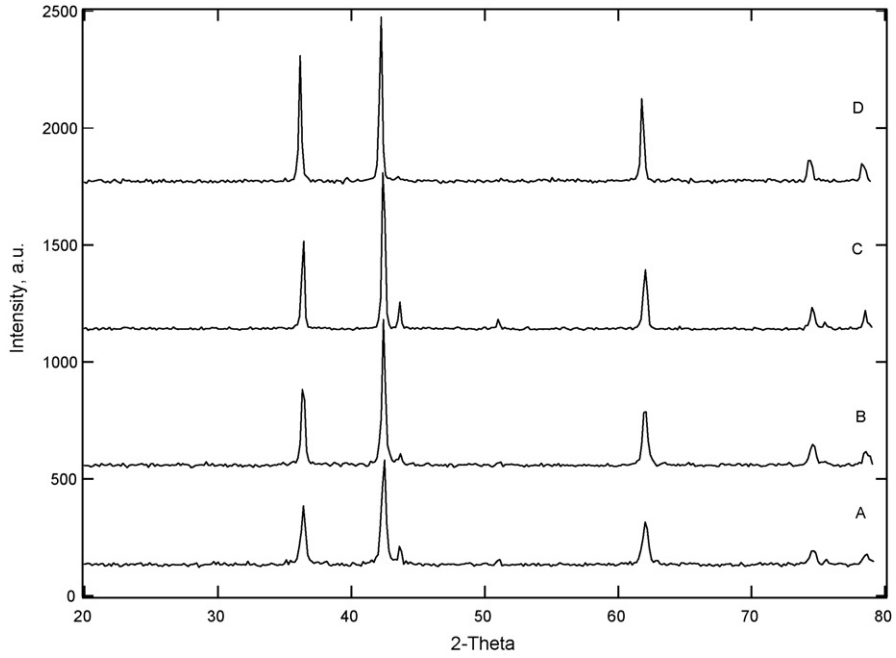

Fig. 5. XRD of the prepared samples obtained by different calcination temperatures, °C; calcination temperature: (A) 550 °C, (B) 650 °C, (C) 750 °C, and (D) 850 °C.

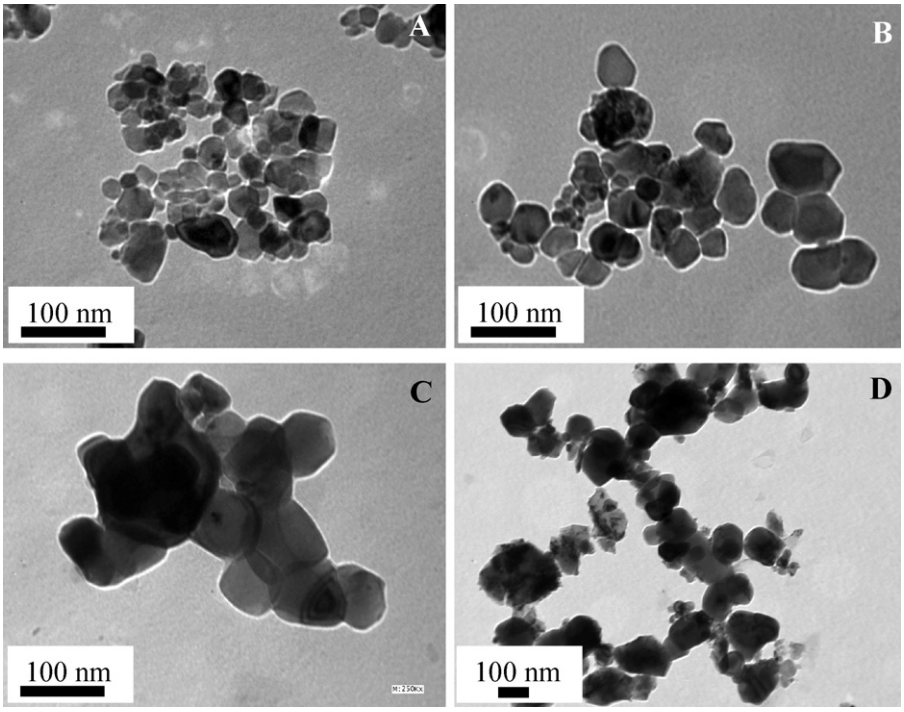

Fig. 6. TEM images of the prepared samples obtained by different calcination temperatures, °C; calcination temperature: : (A) 550 °C, (B) 650 °C, (C) 750 °C, and (D) 850 °C.

Table 3
Effect of calcination temperature on the percentage and the crystallite size of the formed phases, photocatalytic degradation of EDTA and the measured surface area.

Calcination temperature (°C)	% of formed phases		Crystallite size (nm)	Photocatalytic degradation of EDTA (%)	BET (m^2/g)
	NiO	Ni			
550	94.4	5.6	61.8	92.1	99.5
650	97.1	2.9	90.4	90.5	82.5
750	70	30.0	95.0	85.8	61.0
850	100	0.0	101.7	80.4	42.0

Table 4
Magnetic properties of the catalyst prepared at different calcination temperatures.

Calcination temperature (°C)	Magnetic properties			
	Saturation magnetization, M_s (emu/g)	Remanent magnetization, M_r (emu/g)	Coercivity, H_c (Oe)	Remanence ratio, M_r/M_s
550	45.34	1.471	6.463	0.0324
650	38.64	0.7726	3.972	0.0199
750	20.81	0.7393	8.517	0.0355
850	–	–	–	–

coercively and high remnant magnetization. Also, the surface area was found to decrease from 99.5, 82.5, 61.0 and 42.0 m^2/g by increasing the calcination temperature from 550, 650, 750 and 850 °C, see Table 3. Therefore the optimum condition for calcination temperature to prepare our magnetic photocatalyst is 550 °C at which 99.5 m^2/g BET surface area, 45.34 emu/g saturation magnetization, 1.471 emu/g remanent magnetization and 6.463 Oe coercivity were achieved.

3.3.2. Calcined samples and photocatalytic degradation of EDTA

This section is devoted to understand the effect of calcination temperature on the catalytic performance of the as-formed catalysts for EDTA degradation. A series of experiments was conducted accordingly under the following conditions: 0.4 g/l catalyst/EDTA solution ratio; 5×10^{-3} M EDTA; 1 h reaction time and at pH 3. The results are summarized in Table 3. The results indicate that increasing calcination temperature in the order 550, 650, 750, and 850 °C leads to a decrease in EDTA removal efficiency from 92.1, 90.5, 85.8 and 80.4%, respectively. This can be attributed to a decrease in BET values from 99.5, 82.5, 61.0 and 42.0 m^2/g, respectively. Based on this result, the most appropriate calcination temperature is 550 °C at which the prepared catalyst has 99.5 m^2/g BET surface area, 3.44 eV band gap, 94.4% NiO and 92.1% EDTA removal efficiency.

3.4. Parameters of photocatalytic process

3.4.1. Effect of pH

A series of experiments has been carried out to study the effect of pH on EDTA removal efficiency under the following conditions: 0.4 g/l catalyst/EDTA solution ratio; 5×10^{-3} M EDTA and 1 h reaction time. The obtained results indicate that increasing the pH of EDTA solution from 3 to 7 leads to an increase in EDTA removal efficiency from 92.1 to 97.1%, however by exceeding the pH 7, the EDTA removal efficiency almost remains unchanged. The possible reason for this behavior is that alkaline pH value favors the formation of more OH radical due to the presence of large quantity of OH^- ions in the alkaline medium, which enhances the photocatalytic degradation of EDTA significantly [50]. The optimum condition for pH is 7 at which a value of 97.1% photodegradation of EDTA is achieved.

3.4.2. Effect of EDTA concentration

The effect of EDTA concentration on EDTA removal efficiency operating under the above conditions at pH 7 was investigated. The results indicate that an increase in EDTA concentration from 5×10^{-5} to 5×10^{-3} M has no significant effect on EDTA removal efficiency, while at a concentration more than 5×10^{-3} M, the EDTA removal efficiency was significantly decreased. Values of EDTA removal efficiency of 97.1, 80.0, and 50.0% are respectively obtained at EDTA concentrations of 5×10^{-3}, 7.5×10^{-3} and 5×10^{-2} M. The optimum condition for EDTA concentration is 5×10^{-3} M at EDTA removal efficiency of 97.1%.

3.4.3. Effect of catalyst/EDTA solution ratio

Fig. 7 depicts the results representing the effect of catalyst/EDTA solution ratio on EDTA removal efficiency under aforementioned conditions at EDTA concentration 5×10^{-3} M. The results indicate that an increase in catalyst/EDTA solution ratio from 0.2 to 0.4 g/l, leads to an increase in EDTA removal efficiency from 97.1 to 99.9% respectively, whereas at a catalyst/EDTA solution ratio more than 0.4 g/l, the EDTA removal efficiency almost remains unchanged. The optimum condition of catalyst/EDTA solution ratio is 0.4 g/l giving a value of 99.9% EDTA removal efficiency.

Table 5
Rate constant of reaction kinetics of EDTA with Ni/NiO sample.

Catalyst/EDTA solution ratio (g/l)	K ($\times 10^{-4}$ min^{-1})	$t_{1/2}$ (min)
0.2	190	36.5
0.3	222	31.2
0.4	460	15.1
0.6	579	11.9

3.4.4. Kinetics of EDTA with Ni/NiO catalyst

The reaction order with respect to EDTA was determined by plotting the reaction time vs. log[EDTA] according to the following equation for various ratios of catalyst/EDTA solution.

$$\mathrm{Log}[C]_t = -kt + \mathrm{Log}[C]_0$$

$$t_{1/2} = \frac{0.693}{k}$$

where $[C]_0$ and $[C]_t$ represent the concentration of the substance in solution at zero time and t time of illumination respectively, and k and $t_{1/2}$ represent the apparent rate constant (min^{-1}) and half life time of the reaction (min), respectively. The findings are illustrated in Fig. 8 and the apparent rate constants and $t_{1/2}$ are summarized in Table 5. The results show that the reaction follows first order kinetics with respect to EDTA and the rate constants ranged from 190×10^{-4} to 579×10^{-4} min^{-1}. In addition, $t_{1/2}$ was found to decrease from 36.5 to 11.9 min by increasing catalyst/EDTA solution ratio from 2×10^{-4} to 6×10^{-4}. The first order rate equation for EDTA is given by: $R = k[\mathrm{EDTA}]$.

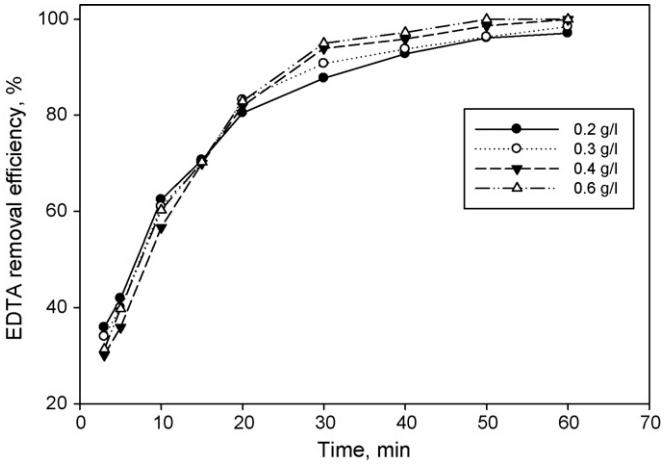

Fig. 7. Effect of catalyst concentration, g/l on EDTA removal efficiency.

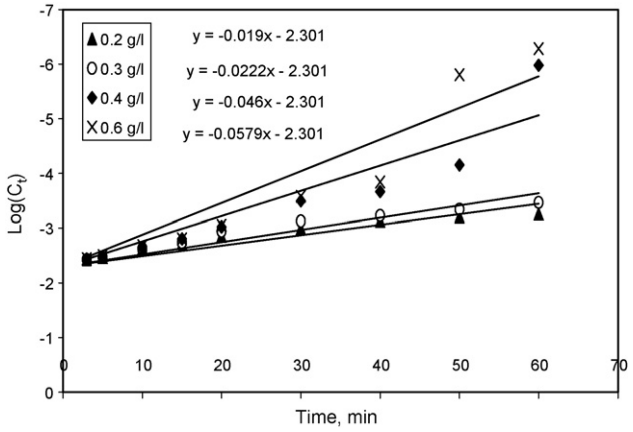

Fig. 8. Reaction kinetic of EDTA.

4. Conclusions

A simple sol–gel approach was employed successfully to synthesize magnetic nanoparticles of Ni/NiO with controlled composition and phase. The as-formed catalyst with and without heat treatment was tested for EDTA degradation in an aqueous solution. Based on the results obtained, it can be concluded that controlling the molar ratio of nickel nitrate/citric acid used during the synthesis process is a key factor for obtaining required catalyst composition and phase. Furthermore, the annealing process is an essential step that greatly influenced the catalyst performance. The obtained EDTA removal efficiency was 99.9% at 5×10^{-3} M EDTA. The reaction of Ni/NiO with EDTA was found to follow first order kinetics with respect to EDTA. The rate constant and $t_{1/2}$ for Ni/NiO at 0.4 g/l catalyst/EDTA solution ratio were, respectively 460 min^{-1}, 15.1 min.

References

[1] A.G.S. Mani, K. Paramasivan, S. Chitra, P.K. Sinha, K.B. Lal, Proceedings of the Indian Environmental Congress, 2004, pp. 276–280.
[2] K. Rosikova, J. John, E. Danacikova-Popelova, F. Sobesta, E.W. Hooper, Proceedings of the Fourth Institute of International Cooperative Environmental Research Florida, Florida State University, Tallahassee, 1998, pp. 379–385.
[3] M.L. Hinck, J. Ferguson, J. Puhaakka, Water Sci. Technol. 35 (1997) 25.
[4] H.J. Brauch, S. Schullerer, Vom Wasser 69 (1987) 155.
[5] H.J. Brauch, S. Schullerer, Vom Wasser 72 (1989) 23.
[6] E. Gilbert, S. Hoffmann-Glewe, Water Res. 24 (1990) 39.
[7] Z. Aksu, J. Yener, Process Biochem. 33 (1999) 649.
[8] M.A. Fox, M.T. Dulay, Chem. Rev. 93 (1993) 341.
[9] P.V. Kamat, Chem. Rev. 267 (1993) 93.
[10] D.F. Ollis, E. Pellizetti, N. Serpone, Environ. Sci. Technol. 25 (1991) 1623.
[11] J. Xu, Y. Ao, M. Chen, D. Fu, J. Alloys Compd. 484 (2009) 73.
[12] H.-F. Yu, S.-T. Yang, J. Alloys Compd. 492 (2010) 695.
[13] K.V. Baiju, P. Periyat, P. Shajesh, W. Wunderlich, K.A. Manjumol, V.S. Smitha, K.B. Jaimy, K.G.K. Warrier, J. Alloys Compd. (2010), doi:10.1016/j.jallcom.2010.06.028.
[14] N. Kaneva, I. Stambolova, V. Blaskov, Y. Dimitriev, S. Vassilev, C. Dushkin, J. Alloys Compd. 500 (2010) 252.
[15] R.M. Mohamed, A.A. Ismail, I. Othman, I.A. Ibrahim, J. Mol. Catal. A 238 (2005) 151.
[16] R.M. Mohamed, I.A. Mkhalid, J. Alloys Compd. 501 (2010) 143.
[17] R.M. Mohamed, I.A. Mkhalid, J. Alloys Compd. 501 (2010) 301.
[18] H.D. Mansilla, C. Bravo, R. Ferreyra, M.I. Litter, W.F. Jardim, C. Lizama, J. Freer, J. Fernández, J. Photochem. Photobiol. A: Chem. 181 (2006) 188.
[19] H. Seshadri, S. Chitra, K. Paramasivan, P.K. Sinha, Desalination 232 (2008) 139.
[20] M.C. Yeber, C. Soto, R. Riveros, J. Navarrete, G. Vidal, Chem. Eng. J. 152 (2009) 14.
[21] J. Wu, X. Lü, L. Zhang, Y. Xia, F. Huang, F. Xu, J. Alloys Compd. 496 (2010) 234.
[22] B. Sheela, H. Gomathi, G.P. Rao, J. Electroanal. Chem. 394 (1995) 267.
[23] M. Chigane, M. Ishikawa, J. Chem. Soc. Faraday Trans. 88 (1992) 2203.
[24] Zh. Jiao, M. Wu, Zh. Qin, H. Xu, Nanotechnology 14 (2003) 458.
[25] M. Kitao, K. Izawa, K. Urabe, T. Komatsu, S. Kuwano, S. Yamada, Jpn. J. Appl. Phys. 33 (1994) 6656.
[26] K. Yoshimura, T. Miki, S. Tanemura, Jpn. J. Appl. Phys. 34 (1995) 2440.
[27] P. Tomczyk, G. Mordarski, J. Oblakowski, J. Electroanal. Chem. 353 (1993) 177.
[28] C.R. Makkus, K. Hemmes, D.W. Wir, J. Electrochem. Soc. 141 (1994) 3429.
[29] B.C. Alcock, Z. Li, W.J. Fergus, L. Wang, Solid State Ionics 39 (1992) 53.
[30] H. Kumagai, M. Matsumoto, K. Toyoda, M. Obara, J. Mater. Sci. Lett. 15 (1996) 1081.
[31] F.F. Ferreira, M.H. Tabacniks, M.C.A. Fantini, I.C. Faria, A. Gorenstein, Solid State Ionics 86–88 (1996) 971.
[32] J. Scarminio, A. Urbano, B.J. Gardes, A. Gorenstein, J. Mater. Sci. Lett. 562 (1992) 11.
[33] M.C.A. Fantini, G.H. Benerra, C.R.C. Carvalho, A. Gorenstein, Proc. SPIE 1536 (1996) 81.
[34] N. Ozer, C.M. Lampert, Proceedings of the 5th World Congress on Chemical Engineering AIChI, New York, 1996, p. 933.
[35] A. Surca, B. Orel, B. Pihlar, J. Sol–Gel Sci. Technol. 8 (1997) 743.
[36] W. Wang, Y. Liu, C. Xu, C. Zheng, G. Wang, Chem. Phys. Lett. 362 (2002) 119.
[37] Y. Lin, T. Xie, B. Cheng, B. Geng, L. Zhang, Chem. Phys. Lett. 380 (2003) 521.
[38] C. Xu, K. Hong, S. Liu, G. Wang, X. Zhao, J. Cryst. Growth 255 (2003) 308.
[39] Y. Zhan, C. Zheng, Y. Liu, G. Wang, Mater. Lett. 57 (2003) 3265.
[40] M.A. Gondal, M.N. Sayeed, A. Alarfaj, Chem. Phys. Lett. 445 (2007) 325.
[41] H. Shu, J. Xie, H. Xu, H. Li, Z. Gu, G. Sun, Y. Xu, J. Alloys Compd. 496 (2010) 633.
[42] Y.-J. Lin, Y.-H. Chang, G.-J. Chen, Y.-S. Chang, Y.-C. Chang, J. Alloys Compd. 479 (2009) 785.
[43] Y. Li, S. Yao, W. Wen, L. Xue, Y. Yan, J. Alloys Compd. 491 (2010) 560.
[44] C.W. Schlapfer, N.N. Vlasova, S.K. Poznyak, A.I. Kokoring, J. Colloid Interface Sci. 239 (2001) 200.
[45] W.E. Mahmoud, H. El-Mallah, J. Phys. D: Appl. Phys. 42 (2009) 035502.
[46] G. Boschloo, A. Hagfeldt, J. Phys. Chem. B 105 (2001) 3039.
[47] T. Tsuboi, W. Kleeman, J. Phys. Condens. Matter 6 (1994) 8625.
[48] J. Miaoa, H. Wanga, Y. Lia, J. Zhu, J.-J. Zhu, J. Cryst. Growth 281 (2005) 525.
[49] F. Rouquerol, J. Rouquerol, K. Sing, Adsorption by Powders and Porous Solids: Principles, Methodology and Applications, Academic Press, San Diego, 1999.
[50] S. Sakthivel, B. Neppolian, M.V. Shankar, B. Arabindoo, M. Palanichamy, V. Murugesan, Solar Energy Mater. Solar Cells 77 (2003) 65.